THE JOURNAL OF BIOLOGICAL CHEMISTRY VOL. 282, NO. 24, pp. 17658–17664, June 15, 2007
Printed in the U.S.A.

Selective Perturbation of the Myosin Recovery Stroke by Point Mutations at the Base of the Lever Arm Affects ATP Hydrolysis and Phosphate Release*

Received for publication, February 19, 2007, and in revised form, April 19, 2007 Published, JBC Papers in Press, April 21, 2007, DOI 10.1074/jbc.M701447200

András Málnási-Csizmadia[‡§], Judit Tóth[‡¶], David S. Pearson[‖], Csaba Hetényi[‡1], László Nyitray[‡], Michael A. Geeves[‖], Clive R. Bagshaw[§], and Mihály Kovács[‡§¶2]

From the [‡]Department of Biochemistry, Eötvös University, H-1117 Budapest, Hungary, [§]Department of Biochemistry, University of Leicester, Leicester LE1 7RH, United Kingdom, [¶]Laboratory of Molecular Physiology, NHLBI, National Institutes of Health, Bethesda, Maryland 20892, and [‖]Department of Biosciences, University of Kent, Canterbury, Kent CT2 7NJ, United Kingdom

After ATP binding the myosin head undergoes a large structural rearrangement called the recovery stroke. This transition brings catalytic residues into place to enable ATP hydrolysis, and at the same time it causes a swing of the myosin lever arm into a primed state, which is a prerequisite for the power stroke. By introducing point mutations into a subdomain interface at the base of the myosin lever arm at positions Lys[84] and Arg[704], we caused modulatory changes in the equilibrium constant of the recovery stroke, which we could accurately resolve using the fluorescence signal of single tryptophan *Dictyostelium* myosin II constructs. Our results shed light on a novel role of the recovery stroke: fine-tuning of this reversible equilibrium influences the functional properties of myosin through controlling the effective rates of ATP hydrolysis and phosphate release.

Various steps of the myosin mechanochemical cycle are linked to large conformational changes of the motor domain, which contains the actin and ATP binding sites as well as the converter region that forms the base of the extended lever arm domain. The converter/lever arm module is thought to amplify the structural changes occurring at the ATPase active site to produce a large working stroke (1, 2).

Upon interacting with ATP, the motor domain undergoes a crystallographically identified large structural rearrangement before hydrolysis takes place. During this transition, the movement of the switch-2 loop of the active site toward the γ-phosphate of ATP brings catalytically important residues to their active positions. This open-closed transition of switch-2 is coupled to a large rotation of the lever arm (from *down* to a primed *up* state), and thus the conformational rearrangement has been termed the recovery stroke, which constitutes the priming of the myosin head in an actin-detached state. Rebinding of myosin to actin in the post-recovery (*up*) conformation is a prelude to the power stroke and force generation (3).

Kinetic studies on a *Dictyostelium* myosin II motor domain construct containing a single ATP-sensitive tryptophan sensor (W501+ located in the relay-converter module) have revealed the correspondence between identified structural states and ATPase intermediates (4, 5). In the model shown in Reaction 1, ATP binding to *apo*-myosin (M^{apo})[3] (K_1k_2) is followed by the recovery stroke (K_{3a}), which is reversible and rapid compared with the subsequent hydrolysis step (K_{3b}). Following hydrolysis, the reversal of the recovery stroke (K_4) is thought to occur before the actual release of P_i (k_5). Reaction 1 and the current study deals with the myosin ATPase in the absence of actin, where lever arm motions are uncoupled from the performance of external work. ADP release (K_6K_7) occurs practically as a reversal of the ATP binding process. (Reaction 1 ignores possible protein structural and/or dynamic differences between the M^{down}·ATP, M^{down}·ADP, and M^{down}·ADP·P_i states.)

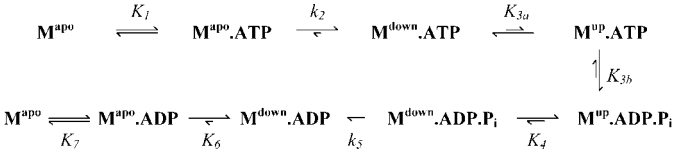

REACTION 1

The above mechanism gives rise to the hypothesis that a shift in the equilibrium constant of the recovery stroke (K_{3a}) will have an effect on the apparent rate constant of ATP hydrolysis (because $^{app}k_H = k_{3b}K_{3a}/(1+K_{3a}) + k_{-3b}$). Furthermore, because P_i release is thought to occur in the switch-2 open (*down*) conformation, the reversal of the recovery stroke (K_4) may influence the steady-state ATPase rate, which is controlled by the effective rate of P_i release. Thus, besides its role in ATP hydrolysis and priming the myosin head, the recovery stroke may be important in fine-tuning the steady-state distribution of myosin molecules in *up* and *down* lever arm orientations and, in

* This work was supported by Wellcome Trust IRDA (071525), National Office for Research and Technology RET 14/2005, and the EMBO/HHMI YIP Programme (to A. M. C.), OTKA Grant TS49812 (to A. M. C. and L.N.), Wellcome Trust Grant 070021 (to M. A. G.), Wellcome Trust and Biotechnology and Biological Sciences Research Council grants (to C. R. B.), and National Institutes of Health Research Grant D43 TW006230 (1 R01 TW007241–01, funded by the Fogarty International Center and the NHLBI, National Institutes of Health), an EMBO-HHMI startup grant, and the Bolyai fellowship of the Hungarian Academy of Sciences (to M. K.). The costs of publication of this article were defrayed in part by the payment of page charges. This article must therefore be hereby marked "*advertisement*" in accordance with 18 U.S.C. Section 1734 solely to indicate this fact.

[1] Present address: Institute of Chemical Physics, University of Tartu, Jakobi 2, 51014 Tartu, Estonia.

[2] To whom correspondence should be addressed: Dept. of Biochemistry, Eötvös University, H-1117 Budapest, Pázmány P. sétány 1/C, Hungary. Tel.: 36-1-381-2171; Fax: 36-1-381-2172; E-mail: kovacsm@elte.hu.

[3] The abbreviation used is: M, myosin; TES, 2-{[2-hydroxy-1,1-bis (hydroxymethyl)ethyl]amino}ethanesulfonic acid.

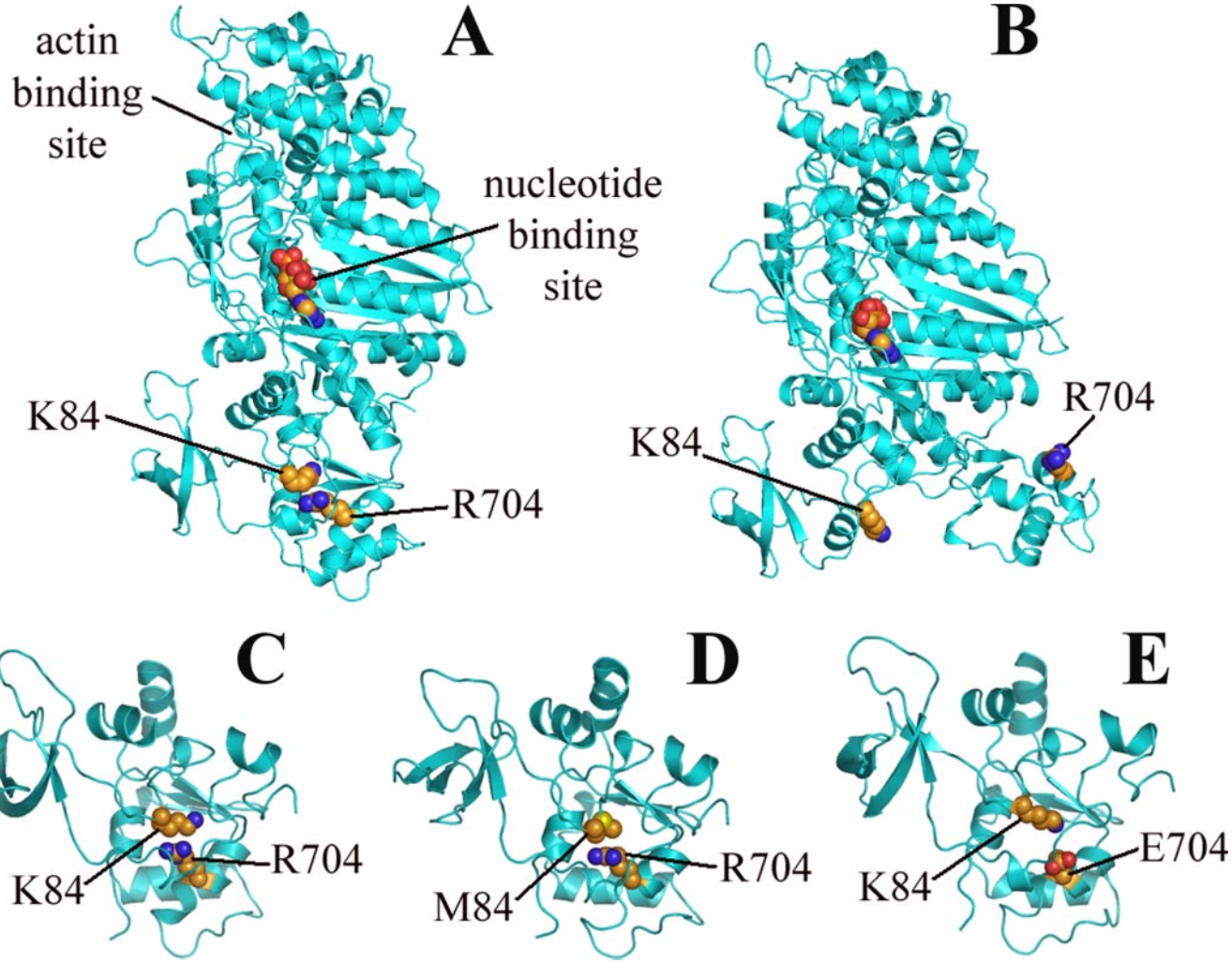

FIGURE 1. *A* and *B*, location of residues 84 and 704 in the *down* (*A*) and *up* (*B*) structures of the myosin motor domain (Protein Data Bank structures 1FMW and reconstituted 1VOM, respectively) (21, 22). The nucleotide and actin binding regions show little change on the recovery stroke. *C–E*, close-up views of the 84–704 interaction in the energy-minimized structure of the wild-type (*C*), K84M (*D*), and R704E (*E*) constructs.

turn, the strong and weak actin binding states during the contractile cycle.

To test this hypothesis, we designed *Dictyostelium* myosin II motor domain mutants to perturb the recovery stroke selectively. This step is accompanied by a large rotation of the converter region that causes disruption of its interface to the N-terminal subdomain of the myosin head (Fig. 1, *A* and *B*). One good candidate for a directed change in the interaction pattern of this interface is the Lys^{84} (N-terminal subdomain)-Arg^{704} (converter) residue pair. In the *down* (pre-recovery) conformation the two side chains, unusually, run almost parallel to each other and their positive charges are separated by only ~0.5 nm (Fig. 1*A*). In the *up* (post-recovery) structure this complex is disrupted (Fig. 1*B*), implying that the introduction of site-directed substitutions in these positions will possibly affect the recovery stroke equilibrium constant. We constructed and characterized the K84M point mutant in which the positive charge of Lys^{84} was removed and the side chain replaced by a roughly isosteric one and R704E in which we intended to convert the originally repulsive Lys^{84}-Arg^{704} interaction into a salt bridge. We introduced these point mutations into the W501+ single tryptophan construct, which has been shown to enable very sensitive resolution of the recovery stroke, while retaining essentially identical kinetic properties to the wild-type enzyme (4, 5). In later sections we will refer to the W501+ control as "wild-type" for simplicity.

EXPERIMENTAL PROCEDURES

Protein Expression and Purification—All constructs used in this study are derivatives of the M761 *Dictyostelium* myosin II motor domain (6). Construction of the plasmid for the W501+ motor domain containing the point mutations W36F, W432F, and W584F was described earlier (4). The W501+ construct was further mutagenized to yield the K84M and R704E mutants as described previously (7). The pDXA-3H expression vector was used for constitutive expression of the motor domains (8). *Dictyostelium* AX3 cells were transformed and cultured and the recombinant proteins were prepared as described previously (4). Protein concentrations were determined using Bradford reagent (Sigma). Purity of the preparations (>95%) was checked by 9% SDS-PAGE.

Nucleotides and Nucleotide Analog Complexes—ATP (special quality, vanadate-free) was from Roche Applied Science. Other nucleotides were purchased from Sigma. The

M·ADP·BeF_x complex was prepared by incubation of 5–20 μM motor domain, 50 μM ADP, 3 mM NaF, 50 μM $BeCl_2$ for 30 min. The M·ADP·AlF_4 complex was made similarly but with 50 μM $AlCl_3$ instead of $BeCl_2$ and incubation for at least 2 h.

Kinetic and Spectroscopic Measurements—All measurements were carried out in a buffer comprising 20 mM TES, pH 7.5, 40 mM NaCl, and 2 mM $MgCl_2$ as described previously (4, 5, 9). Reaction profiles were analyzed by fitting to exponential functions using Origin v7.5 (Microcal Software).

Molecular Dynamics Simulations—Protein Data Bank structure 1FMW and its single point mutants were used as inputs in the modeling studies. Energy minimization and subsequent 5-ns molecular dynamics equilibration were performed with the GROMACS program package (10). 17800 explicit water molecules surrounded the proteins during calculations.

RESULTS

Structural Integrity of the Mutants—Molecular dynamics simulations of the wild-type and mutant proteins in a water box showed that the amino acid substitutions did not cause significant structural changes even in the vicinity of the targeted side chains and that the structures were stable over a 5-ns time scale (Fig. 1, *C–E*). The charge separation between Lys^{84} and Glu^{704} in the R704E mutant was rather similar to that between Lys^{84} and Arg^{704} of the wild-type enzyme (0.5 nm). Also, the side chain of Met^{84} in the K84M mutant adopted a very similar conformation to the corresponding Lys^{84} of the wild-type construct and had a similar proximity to Arg^{704}.

Steady-state ATPase Activities—The basal (actin-free) steady-state ATPase activity of K84M was ~1.5 times, and that of R704E was ~3 times, higher than that of the wild-type construct (Table 1). In addition to the NADH-linked assay, ATPase activities were confirmed by multiple turnover tryptophan fluorescence (as described in Ref. (4), data not shown).

Tryptophan Fluorescence Changes on Nucleotide Interaction—In our earlier studies, W501 showed a small quench on ADP binding (transition from *apo* to *down* conformation), whereas ATP binding caused a large fluorescence increase as the *up* state became populated (4, 5, 11) (Reaction 1). Fig. 2 shows tryptophan fluorescence emission spectra of the studied constructs in the absence of nucleotide, and in ADP and ATP. The extent of the quench caused by ADP was similar in all constructs, whereas the fluorescence increase on ATP addition was markedly smaller in R704E than in the other two constructs. The blue shifts characteristic of both ADP and ATP binding to *apo*-W501+ were not affected by the mutations (Fig. 2).

We measured the temperature dependence of the tryptophan fluorescence emission of the studied constructs (Fig. 3, *A–C*). The slope of the temperature dependence of the wild-type construct in the absence of nucleotide, in ADP, and ADP·AlF_4 (an ADP·P_i analog) was similar to that of free tryptophan, implying that the motor domain adopts three distinct conformations with different fluorescence intensities in these cases (*apo* in the absence of nucleotide, *down* in ADP, and *up* in ADP·AlF_4) (Fig. 3*A*) (5). The temperature dependence was clearly different in ATP and in the ATP analogs ADP·BeF_x and AMPPNP. The intermediate intensities and markedly different slopes in these cases have been interpreted by means of the formation of a temperature-dependent reversible equilibrium of the *down* and *up* states, *i.e.* the recovery stroke (Fig. 3*A*) (5).

TABLE 1
Kinetic and thermodynamic properties of motor domain constructs
Rate and equilibrium constants are based on Reaction 1.

	T	Wild-type[a]	K84M	R704E
	°C			
Steady-state basal ATPase activity (s^{-1})	20	0.05 ± 0.01	0.08 ± 0.01	0.17 ± 0.03
ATP binding and hydrolysis				
K_1k_2 (μM^{-1} s^{-1})	20	1.1	0.94	1.1
$^{app}K_H$ (s^{-1})[b]	5	3.4 ± 0.1	2.0 ± 0.03	1.8 ± 0.01
$^{app}K_H$ (s^{-1})[b]	20	32 ± 1	17 ± 0.2	12 ± 0.1
Recovery stroke				
AMPPNP				
K_{3a}[c]	10	0.13 ± 0.04	0.04 ± 0.02	0.02 ± 0.00
K_{3a}[c]	25	0.76 ± 0.30	0.28 ± 0.04	0.10 ± 0.01
ΔH^0_{3a} (kJ mol^{-1})[d]		82 ± 29	95 ± 23	89 ± 6
ΔS^0_{3a} (kJ mol^{-1} K^{-1})[d]		0.27 ± 0.10	0.31 ± 0.08	0.26 ± 0.02
ADP·BeF_x				
K_{3a}[c]	10	0.27 ± 0.02	0.20 ± 0.02	0.11 ± 0.04
K_{3a}[c]	25	1.4 ± 0.3	0.80 ± 0.01	0.40 ± 0.04
ΔH^0_{3a} (kJ mol^{-1})[d]		74 ± 10	67 ± 6	71 ± 21
ΔS^0_{3a} (kJ mol^{-1} K^{-1})[d]		0.25 ± 0.04	0.22 ± 0.02	0.23 ± 0.07
ADP binding and release				
k_{-6}/K_7 (μM^{-1} s^{-1})[e]	20	1.8	0.82	1.5
K_7 (μM)[e]	20	460 ± 110	450 ± 100	400 ± 30
k_{-6} (s^{-1})[e]	20	850 ± 90	370 ± 30	580 ± 20
k_6 (s^{-1})[f]	20	7.9	8.8	5.2
$1/K_6$	20	110	42	110
K_{eq} (μM)[g]	20	4.2	8.8	5.3

[a] W501+ construct (see Introduction).
[b] Apparent rate constant of the ATP hydrolysis step (see "Results").
[c] Calculated from tryptophan fluorescence intensities as $K_{3a} = (F_x - F_{down})/(F_{up} - F_x)$ where F_{down} and F_{up} are the fluorescence intensities in the *down* (ADP-bound) and *up* (ADP·AlF_4-bound) states, respectively, and F_x is the intensity of the given nucleotide analog complex (Fig. 3, *A–C*).
[d] Calculated from the van't Hoff plots of the recovery stroke ($\ln K_{3a} = -\Delta H^0_{3a}/RT + \Delta S^0_{3a}/R$; Fig. 3, *D* and *E*).
[e] Calculated from the hyperbolic dependence of the k_{obs} of ADP binding transients on [ADP] ($k_{obs} = k_{-6}[ADP]/(K_7+[ADP]) + k_6$; Fig. 6*A*).
[f] From ADP chasing experiments (Fig. 6*B*).
[g] Equilibrium dissociation constant of ADP binding ($K_{eq} = K_6K_7$).

In the *apo*, ADP (*down*), and ADP·AlF_4 (*up*) states, the K84M and R704E constructs showed similar profiles to those of the wild type, indicating that the gross structures of these states are unchanged by the mutations (Fig. 3, *A–C*). For ADP·BeF_x and AMPPNP, the equilibrium constant of the recovery stroke (K_{3a}) could be calculated from fluorescence intensities as $K_{3a} = (F_x - F_{down})/(F_{up} - F_x)$ where F_x, F_{down}, and F_{up} are fluorescence intensities in the presence of the given nucleotide, ADP (*down* state), and ADP·AlF_4 (*up* state), respectively. The equilibrium parameters showed that the K84M mutation, and even more so the R704E mutation, caused marked shifts in favor of the *down* conformation (Table 1). In ATP the situation is more complex because the apparent equilibrium constant of the recovery stroke ($^{app}K_{3a}$) is also affected by the hydrolysis step ($^{app}K_{3a} = K_{3a}(1 + K_{3b})$, Reaction 1), but a shift toward the *down* state in R704E is evident even in this case (Fig. 3, *A–C*).

Although the mutations shifted the equilibrium constant of the recovery stroke (K_{3a}) several times, these have only small perturbations in the overall energetic profile of this step. The small ΔG_o associated with the recovery stroke is composed of a large enthalpy increase (ΔH_o = 50–100 kJ/mol) and a compensating entropic contribution (Fig. 3, *D* and *E*, Table 1) in all mutants and the wild type.

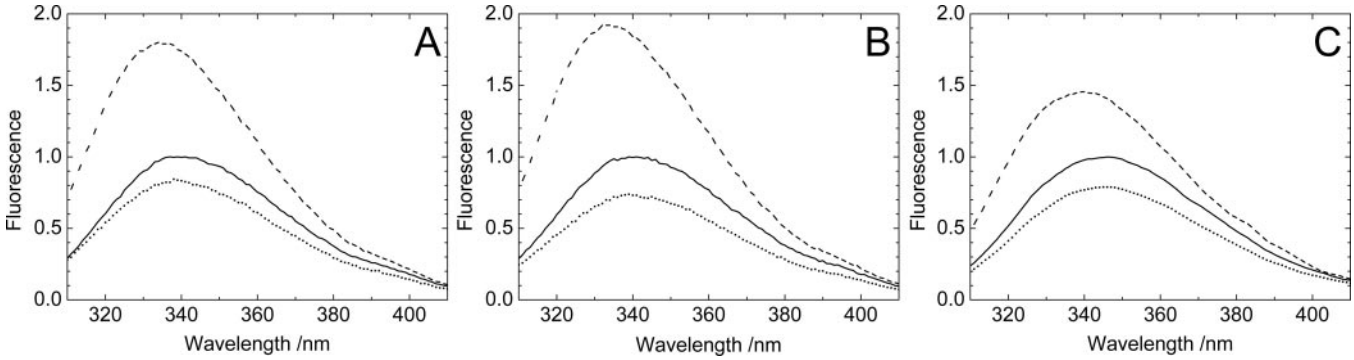

FIGURE 2. **Tryptophan fluorescence emission spectra of the wild-type (*A*), K84M (*B*), and R704E (*C*) constructs in the absence of nucleotide (*solid lines*), in 0. 5 mM ADP (*dotted lines*), and 1 mM ATP (*dashed lines*).** Tryptophan was excited at 297 nm (1-nm bandwidth). Spectra were recorded at 20 °C and normalized to the intensity maximum of the nucleotide-free state.

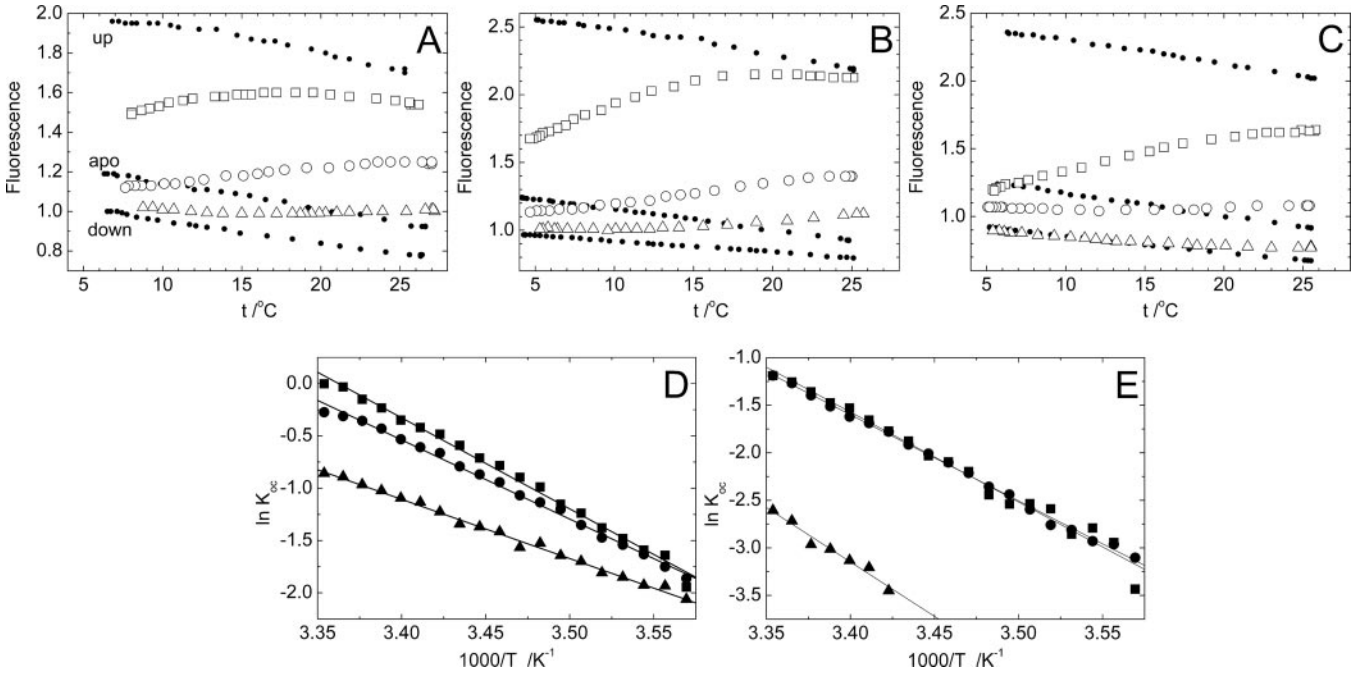

FIGURE 3. *A–C*, temperature dependence of the normalized tryptophan fluorescence intensity of the wild-type (*A*), K84M (*B*), and R704E (*C*) constructs in the absence of nucleotide (data set marked as *apo*), and in ADP (marked as *down*), ADP·AlF_4 (marked as *up*), ATP (*squares*), ADP·BeF_x (*circles*), and AMPPNP (*triangles*). Excitation was at 297 nm (1-nm bandwidth), and the emitted light was selected through a 320-nm-long pass filter. Data were normalized to the intensity of the apo state at 20 °C. *D* and *E*, Van't Hoff plots of the equilibrium constant of the recovery stroke (K_{3a}) of the wild-type (*squares*), K84M (*circles*), and R704E (*triangles*) constructs in ADP·BeF_x (*D*) and AMPPNP (*E*) calculated as described in Table 1.

Kinetics of ATP Interaction—On mixing the W501+ motor domain with ATP in the stopped-flow, the two-step ATP binding process (K_1k_2 in Reaction 1) is followed by the more rapid recovery stroke (K_{3a}) and the subsequent hydrolysis step (K_{3b}) (4, 5). The kinetics of the initial phase of the tryptophan fluorescence transients is dictated by nucleotide binding (K_1k_2), but the amplitude of this phase will be set by the equilibrium constant of the oncoming rapid recovery stroke (K_{3a}). Because the W501 fluorescence intensity in the *down* state is lower and in the *up* state is higher than that in the *apo* state, the initial phase can be either a burst (fluorescence increase) or a quench (fluorescence drop), depending on the value of K_{3a}. After this initial phase, there is a subsequent fluorescence enhancement indicating that the hydrolysis step ($K_{3b} \gg 1$) pulls the reaction over to result in the predominance of the high fluorescence M^{up}·ADP·P_i state (Reaction 1). The observed rate constant (k_{obs}) of this second phase (*i.e.* the apparent rate constant of ATP hydrolysis, $^{app}k_H$) will be a composite of the recovery stroke equilibrium constant and the rate constants of the hydrolysis step ($^{app}k_H = k_{3b}K_{3a}/(K_{3a} + 1) + k_{-3b}$; Reaction 1) (4, 5).

The dependence of the k_{obs} of the initial phase on ATP concentration was quasilinear in all mutants, showing signs of saturation above 1 mM ATP ($K_1 \leq 10^{-3}$ μM^{-1}, data not shown). The plots had slopes (K_1k_2) ~ 0.5 μM^{-1} s^{-1} at 5 °C, and ~1 μM^{-1} s^{-1} at 20 °C, consistent with earlier wild-type data and showing little effect of the mutations on ATP binding kinetics (Table 1) (4). However, a more pronounced initial quench (or a lack of an initial burst) together with a slower second phase (smaller $^{app}k_H$) in the mutants compared with the wild-type demonstrated a marked reduction in the recovery stroke equilibrium constant (K_{3a}) caused by the mutations (Fig. 4, *A* and *B*). Fig. 4*C* shows the k_{obs} of the second phase at 20 °C plotted against ATP concentration. A marked reduction in the maxi-

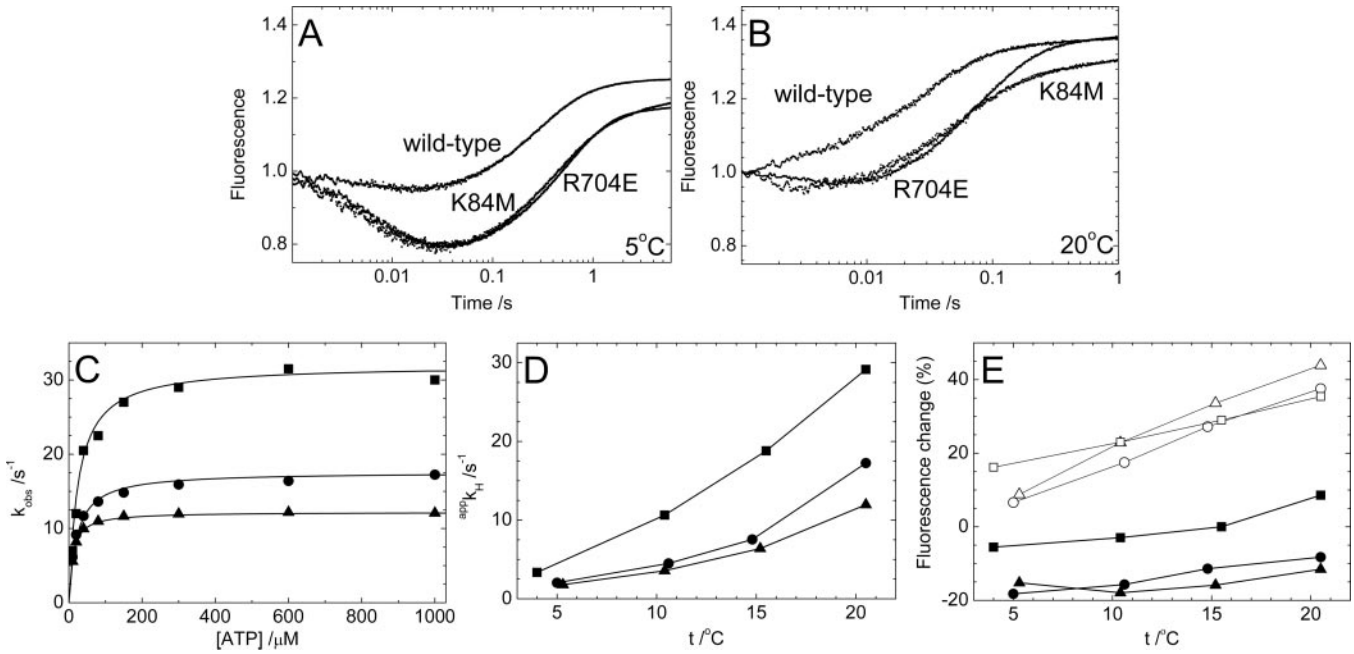

FIGURE 4. *A* and *B*, stopped-flow fluorescence transients recorded on mixing 2 μM wild-type, K84M, and R704E motor domain with 300 μM ATP at 5 °C (*A*) and 20 °C (*B*). Fluorescence intensities were normalized to the initial fluorescence level. *C*, ATP concentration dependence of the observed rate constants (k_{obs}) of the second phase of the reaction of the wild-type (*squares*), K84M (*circles*), and R704E (*triangles*) constructs with ATP at 20 °C. Hyperbolic fits to the data yielded maximal k_{obs} (*i.e.* $^{app}k_H$) values listed in Table 1. *D* and *E*, temperature dependence of $^{app}k_H$ (*D*) and the percentile fluorescence change (relative to the *apo* fluorescence level) after the initial (*E, solid symbols*) and second (*E, open symbols*) phases of the reaction in the wild-type (*squares*), K84M (*circles*), and R704E (*triangles*) constructs.

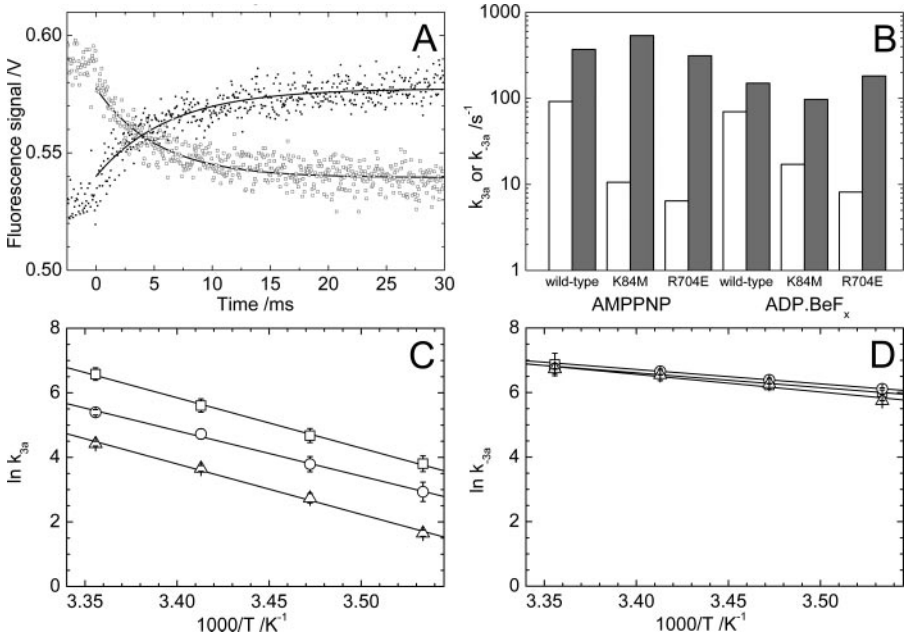

FIGURE 5. *A*, sample tryptophan fluorescence transients of the K84M·ADP·BeF$_x$ complex after a rapid pressure rise (*open symbols*) and pressure drop (*solid symbols*) at 25 °C, characterized by k_{obs} values of 190 and 160 s^{-1}, respectively. *B*, forward (k_{3a}, *white columns*) and reverse (k_{-3a}, *gray columns*) rate constants of the recovery stroke in AMPPNP and ADP·BeF$_x$ at 10 °C. *C* and *D*, Arrhenius plots of k_{3a} (*C*) and k_{-3a} (*D*) in the wild-type (*squares*), K84M (*circles*), and R704E (*triangles*) constructs in AMPPNP. Fitted parameters are listed in Table 2.

mal k_{obs} was observed in K84M and even more in R704E. This tendency held throughout the temperature range studied (5–20 °C, Fig. 4*D*). Analysis of the amplitude data of the stopped-flow transients also highlighted the correspondence between the recovery stroke equilibrium constant (K_{3a}) and the apparent rate constant of the hydrolysis step ($^{app}k_H$). The fluorescence levels after the initial phase were lower in K84M and even more in R704E than in the wild-type (indicating a smaller K_{3a}), whereas in the second phase ATP hydrolysis (K_{3b}) pulled the reaction to the high fluorescence M^{up}·ADP·P_i state in all cases (Fig. 4*E*, Reaction 1).

Kinetics of the Recovery Stroke—Because the recovery stroke is much faster than both the preceding and subsequent steps, its kinetics can be investigated only by its selective perturbation using relaxation kinetic techniques (5, 12). Following a rapid pressure-jump, the motor domain-nucleotide analog (ADP·BeF$_x$ and AMPPNP) complexes showed conformational relaxation of the reversible and pressure-sensitive recovery stroke (Fig. 5*A*). The k_{obs} of these tryptophan fluorescence transients is the sum of the forward and reverse rate constants ($k_{obs} = k_{3a} + k_{-3a}$). k_{3a} and k_{-3a} in the ADP·BeF$_x$ and AMPPNP complexes of the motor domain could thus be determined from the k_{obs} of the pressure-jump records and the K_{3a} equilibrium constants determined in equilibrium fluorescence measurements (Fig. 3, Table 1).

Fig. 5*B* shows that the shift toward the *down* state (a reduction in K_{3a}) caused by the mutations is brought about predominantly by a reduction in k_{3a}, whereas the reverse rate

constant (k_{-3a}) remains largely unaffected. Furthermore, in the Arrhenius plots of these rate constants the slopes of ln k_{3a} or ln k_{-3a} *versus* 1/T were very similar in all constructs, whereas the k_{3a} values of the mutants were markedly offset from those in the wild-type (Fig. 5, *C* and *D*). This means that the mutations caused a reduction in the pre-exponential term of the Arrhenius equation, but the exponential term remained largely unchanged ($k = A \exp(E^{\#}/RT)$ where A is the pre-exponential term and $E^{\#}$ is the activation energy; Table 2).

Kinetics of ADP Binding and Release—On mixing with excess ADP in the stopped-flow, all constructs showed a single exponential quench in tryptophan fluorescence (traces not shown). Analysis of the hyperbolic dependence of k_{obs} on ADP concentration ($k_{obs} = k_{-6}[ADP]/(K_7 + [ADP]) + k_6$) showed that the initial low affinity binding step (K_7) was not affected by the mutations, whereas the rate constant of the subsequent isomerization (k_{-6}) was slightly reduced (Fig. 6*A*, Table 1, Reaction 1).

The rate constants of ADP dissociation (k_6) were determined by chasing experiments in which the motor domain·ADP complexes were mixed with high concentrations of ATP in the stopped-flow (Fig. 6*B*). The mutations had no profound effect on either k_6 or the overall ADP binding equilibrium constant ($K_{eq} = K_7K_6$; Table 2).

TABLE 2
Arrhenius parameters of the recovery stroke

Rate constant[a]	Nucleotide ligand	$E^{\#}$ (kJmol^{-1})[b]	A (s^{-1})[c]	Reduction of *A* in mutants[d]	
				K84M	R704E
k_{3a}	AMPPNP	125 ± 6	9.9×10^{24}	0.15	0.09
	ADP·BeF_x	84 ± 7	2.1×10^{17}	0.21	0.14
k_{-3a}	AMPPNP	37 ± 6	2.6×10^{9}	ND[e]	ND[e]
	ADP·BeF_x	9 ± 4	5.7×10^{3}	ND[e]	ND[e]

[a] Rate constants were extracted from the predominant phase of pressure jump records. They were calculated from the pressure jump k_{obs} ($=k_{3a} + k_{-3a}$) values and the K_{3a} ($=k_{3a}/k_{-3a}$) values calculated from steady-state fluorescence intensities (Figs. 3 and 5, Table I). In some cases, pressure jump relaxations contained minor slow phases of uncertain origin.
[b] Apparent activation energies. Differences between $E^{\#}$ values of the wild-type and mutant constructs were within experimental error. S.E. of all measurements with a given nucleotide are shown.
[c] Pre-exponential factor in the wild-type construct.
[d] Expressed as $A_{mutant}/A_{wild\text{-}type}$.
[e] Not detectable. Differences between wild-type and mutants were within experimental error.

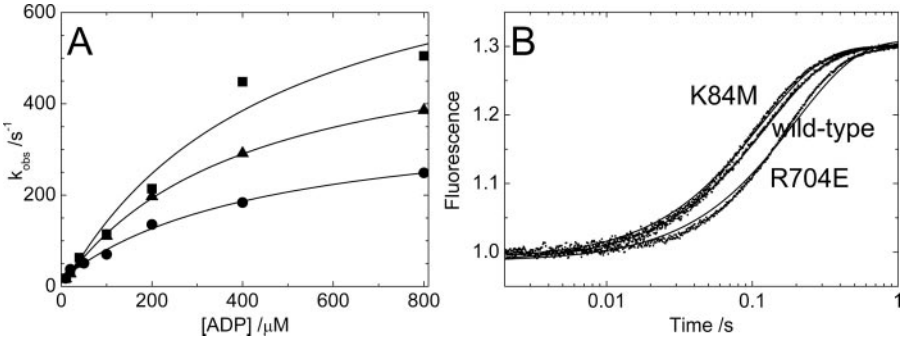

FIGURE 6. *A,* ADP concentration dependence of the k_{obs} of the fluorescence change on mixing 2 μM wild-type (*squares*), K84M (*circles*), and R704E (*triangles*) motor domain with ADP. Data were fitted to a hyperbolic equation and yielded parameters listed in Table 1. *B,* kinetics of ADP dissociation as measured by mixing 2 μM motor domain plus 50 μM ADP with 1 mM ATP in the stopped-flow. Fitted rate constants (k_6) are listed in Table 1. The ADP dissociation traces were not clear single exponentials, but the fitted k_6 values were consistent with K_{eq} calculated from equilibrium fluorescence titrations (data not shown).

DISCUSSION

Selective Perturbation of the Recovery Stroke by Subdomain Interactions—We aimed to selectively perturb the myosin recovery stroke by converting the repulsive Lys^{84}-Arg^{704} interaction into a weak attraction in the K84M mutant and a salt bridge in the R704E construct (Fig. 1). These mutations are located at the N-terminal subdomain-converter interface, which is far from the nucleotide binding pocket. As judged from the kinetics of nucleotide binding to and release from the mutants as well as molecular dynamic simulations, the substitutions did not affect the overall structure of the nucleotide binding site (Fig. 1). However, the mutations had a distinct effect on the recovery stroke that involves marked conformational rearrangements involving distant parts of the molecule. Thus, the studied mutations modulated surface charges sufficiently to have an effect on recovery stroke kinetics, but they did not override the structures of the start and end points of this transition. In all constructs ADP induced the same pre-recovery (switch-2 open or lever arm *down*) state and ADP·AlF_4 induced the post-recovery (switch-2 closed or lever arm *up*) state, as judged by W501 emission intensity (Fig. 3, *A–C*). Other attractive forces across the subdomain interface in the wild type must dominate over the repulsive force between Lys^{84} and Arg^{704} in the *down* state in order to bring them to within 0.5 nm. The wild-type Lys^{84}-Arg^{704} repulsive interaction exists only in the *down* state, and we show that this state becomes more favorable in the order wild-type → K84M → R704E.

It should be noted that the R704E mutation would also disrupt a salt bridge to Glu^{755} within the same subdomain; however, this appears to have little consequence on the overall properties of this construct. In particular, in the K84M mutant where the Arg^{704}-Glu^{755} salt bridge was intact, the kinetic and thermodynamic effects on the recovery stroke were perturbed in the same direction as in the R704E construct.

The Recovery Stroke Is Coupled to ATP Hydrolysis and P_i Release—By characterizing the transient fluorescence profiles of the interaction of the mutants with ATP and their steady-state ATPase activity, we demonstrate that even a moderate decrease in the equilibrium constant of the rapid and reversible recovery stroke causes significant slowing of ATP hydrolysis, which takes place after the recovery stroke (Fig. 4, Table 1, Reaction 1). Conversely, P_i release, which is the rate-limiting step of the basal ATPase cycle and takes place after the reversal of the recovery stroke (K_4), is accelerated by the same mutations (Table 1, Reaction 1). This finding is consistent with earlier work in which trinitropheny-

lation of Lys^{84} caused a marked increase in the basal steady-state ATPase activity of *Dictyostelium* myosin II because the pre-recovery state became predominant during the enzymatic cycle (13).

Mechanism of the Recovery Stroke—We show that the studied mutations selectively decreased the forward rate constant of the recovery stroke (k_{3a}), whereas they did not have a remarkable effect on the reverse rate constant (k_{-3a}) (Fig. 5*B*, Table 2). The structural basis of the asymmetric effect is the disruption of the subdomain interface containing residues 84 and 704 upon the recovery stroke that moves these residues ~3.8 nm apart from each other (Fig. 1, *A* and *B*) (1). Because only a short-range interaction can be formed between these side chains, the mutations do not affect the reverse rate constant (k_{-3b}).

It is surprising that, although the mutations targeted a specific side chain interaction that could be expected to have an enthalpic character, the pre-exponential factor changed rather than the apparent activation energy of the recovery stroke (Fig. 5, *C* and *D*, Table 2). The mutations investigated in the present study affect short-range interactions in the pre-recovery conformation, and therefore they limit the entry into the pathway leading to the conformational change and possibly reshape the diffusion landscape in the initial part of the pathway. The recent simulations of the reaction coordinate of the myosin recovery stroke using Conjugate Peak Refinement provide some indications as to the nature of this pathway (14). Protein conformational changes that gate enzyme activity and protein folding are likely to share these characteristics.

Role of the Recovery Stroke Equilibrium in the Myosin Mechanism—By affecting the effective rate of ATP hydrolysis and P_i release, the equilibrium constant of the recovery stroke may influence the distribution of steady-state enzymatic intermediates during the functioning of myosins. Given the widely varying actin affinities of these intermediates, this effect may also influence the duty ratio, *i.e.* the fractional occupancy of strongly actin-bound myosin states during steady-state ATPase cycling. The duty ratio is a key functional parameter for the effective functioning of different motors. (For instance, ensemble motors such as muscle myosin II exhibit a low duty ratio, whereas single-molecule stepping by myosin V requires a high duty ratio.) Indeed, the ATP hydrolysis step is quite reversible in most myosins examined: the apparent equilibrium constant of the hydrolysis of enzyme-bound ATP ($^{app}K_H$) is between 0.3 and 9 for various myosins (15–20). Because the chemical step is coupled to the recovery stroke (5, 12), the recovery stroke equilibrium constant (K_{3a}) is likely to be a key modulator of $^{app}K_H$ in most cases (in case of quasi-irreversible ATP binding, $^{app}K_H = K_{3a}K_{3b}/(1 + K_{3a} + K_{3a}K_{3b})$; Reaction 1). $^{app}K_H$, in turn, can significantly influence the duty ratio by limiting the rate of entry into the strong binding actomyosin complex. Interestingly, Arg^{704} is highly conserved among at least eight myosin classes (including myosins I, II, and V) whereas Lys^{84} is only conserved within class II myosins (19). Thus, the residues mutated in the current study may even play a role in the functional diversity of myosins, which hypothesis needs further investigation.

REFERENCES

1. Fisher, A. J., Smith, C. A., Thoden, J. B., Smith, R., Sutoh, K., Holden, H. M., and Rayment, I. (1995) *Biochemistry* **34,** 8960–8972
2. Geeves, M. A., and Holmes, K. C. (2005) *Adv. Protein Chem.* **71,** 161–193
3. Zeng, W., Conibear, P. B., Dickens, J. L., Cowie, R. A., Wakelin, S., Malnasi-Csizmadia, A., and Bagshaw, C. R. (2004) *Philos. Trans. R. Soc. Lond. B Biol. Sci.* **359,** 1843–1855
4. Malnasi-Csizmadia, A., Woolley, R. J., and Bagshaw, C. R. (2000) *Biochemistry* **39,** 16135–16146
5. Malnasi-Csizmadia, A., Pearson, D. S., Kovacs, M., Woolley, R. J., Geeves, M. A., and Bagshaw, C. R. (2001) *Biochemistry* **40,** 12727–12737
6. Kurzawa, S. E., Manstein, D. J., and Geeves, M. A. (1997) *Biochemistry* **36,** 317–323
7. Kovacs, M., Toth, J., Malnasi-Csizmadia, A., Bagshaw, C. R., and Nyitray, L. (2004) *J. Muscle Res. Cell Motil.* **25,** 95–102
8. Manstein, D. J., and Hunt, D. M. (1995) *J. Muscle Res. Cell Motil.* **16,** 325–332
9. Pearson, D. S., Holtermann, G., Ellison, P., Cremo, C., and Geeves, M. A. (2002) *Biochem. J.* **366,** 643–651
10. Lindahl, E., Hess, B., and van der Spoel, D. (2001) *J. Mol. Model.* **7,** 306–317
11. Malnasi-Csizmadia, A., Kovacs, M., Woolley, R. J., Botchway, S. W., and Bagshaw, C. R. (2001) *J. Biol. Chem.* **276,** 19483–19490
12. Urbanke, C., and Wray, J. (2001) *Biochem. J.* **358,** 165–173
13. Ajtai, K., Peyser, Y. M., Park, S., Burghardt, T. P., and Muhlrad, A. (1999) *Biochemistry* **38,** 6428–6440
14. Fischer, S., Windshugel, B., Horak, D., Holmes, K. C., and Smith, J. C. (2005) *Proc. Natl. Acad. Sci. U. S. A.* **102,** 6873–6878
15. Bagshaw, C. R., and Trentham, D. R. (1973) *Biochem. J.* **133,** 323–328
16. Kovacs, M., Wang, F., Hu, A., Zhang, Y., and Sellers, J. R. (2003) *J. Biol. Chem.* **278,** 38132–38140
17. Kovacs, M., Wang, F., and Sellers, J. R. (2005) *J. Biol. Chem.* **280,** 15071–15083
18. Ostap, E. M., and Pollard, T. D. (1996) *J. Cell Biol.* **132,** 1053–1060
19. Sellers, J. R. (1999) *Myosins*, Oxford University Press, New York
20. Wang, F., Kovacs, M., Hu, A., Limouze, J., Harvey, E. V., and Sellers, J. R. (2003) *J. Biol. Chem.* **278,** 27439–27448
21. Bauer, C. B., Holden, H. M., Thoden, J. B., Smith, R., and Rayment, I. (2000) *J. Biol. Chem.* **275,** 38494–38499
22. Smith, C. A., and Rayment, I. (1996) *Biochemistry* **35,** 5404–5417